

Article

Geochemical and Volcanological Criteria in Assessing the Links between Volcanism and VMS Deposits: A Case on the Iberian Pyrite Belt, Spain

Emilio Pascual ^{1,*}, Teodosio Donaire ¹, Manuel Toscano ¹, Gloria Macías ¹, Christian Pin ² and Michael Andrew Hamilton ³

¹ Departamento de Ciencias de la Tierra, Universidad de Huelva, 21071 Huelva, Spain; donaire@uhu.es (T.D.); mtoscano@uhu.es (M.T.); gloria.macias@alu.uhu.es (G.M.)

² Département de Sciences de la Terre CNRS, Université Blaise Pascal, 63001 Clermont-Ferrand, France; C.Pin@opgc.univ-bpclermont.fr

³ Department of Earth Sciences, University of Toronto, Toronto, ON M5S 3B1, Canada; mahamilton@es.utoronto.ca

* Correspondence: pascual@uhu.es

Abstract: VMS deposits in the Iberian Pyrite Belt (IPB), Spain and Portugal, constitute the largest accumulation of these deposits on Earth. Although several factors account for their genetic interpretation, a link between volcanism and mineralization is generally accepted. In many VMS districts, research is focused on the geochemical discrimination between barren and fertile volcanic rocks, these latter being a proxy of VMS mineralization. Additionally, the volcanological study of igneous successions sheds light on the environment at which volcanic rocks were emplaced, showing an emplacement depth consistent with that required for VMS formation. We describe a case on the El Almendro–Villanueva de los Castillejos (EAVC) succession, Spanish IPB, where abundant felsic volcanic rocks occur. According to the available evidence, their geochemical features, ϵ Nd signature and U–Pb dates suggest a possible link to VMS deposits. However, (paleo)volcanological evidence here indicates pyroclastic emplacement in a shallow water environment. We infer that such a shallow environment precluded VMS generation, a conclusion that is consistent with the absence of massive deposits all along this area. We also show that this interpretation lends additional support to previous models of the whole IPB, suggesting that compartmentalization of the belt had a major role in determining the sites of VMS deposition.

Keywords: felsic volcanism; petrology; geochemistry; isotope geology; U–Pb dating; VMS deposits; Iberian Pyrite Belt; Spain



Citation: Pascual, E.; Donaire, T.; Toscano, M.; Macías, G.; Pin, C.; Hamilton, M.A. Geochemical and Volcanological Criteria in Assessing the Links between Volcanism and VMS Deposits: A Case on the Iberian Pyrite Belt, Spain. *Minerals* **2021**, *11*, 826. <https://doi.org/10.3390/min11080826>

Academic Editor: Alexander R Cruden

Received: 16 June 2021

Accepted: 22 July 2021

Published: 30 July 2021

Publisher's Note: MDPI stays neutral with regard to jurisdictional claims in published maps and institutional affiliations.



Copyright: © 2021 by the authors. Licensee MDPI, Basel, Switzerland. This article is an open access article distributed under the terms and conditions of the Creative Commons Attribution (CC BY) license (<https://creativecommons.org/licenses/by/4.0/>).

1. Introduction

Volcanogenic massive sulfide (VMS) deposits constitute today one of the major sources of base metals on Earth [1]. These deposits, occurring both in Precambrian and Phanerozoic times, formed in a range of geological settings, most often related in time and space to felsic volcanic rocks within bimodal, mafic–felsic volcanic successions [2–4]. Among VMS areas, the Iberian Pyrite Belt, in the SW Iberian Peninsula, is of great economic interest because it hosts a huge number of sulfide masses, including world-class deposits such as Rio Tinto and Neves Corvo. Moreover, recent exploration has led to the finding of several new economic deposits. The Rio Tinto mining district alone is interpreted as the largest VMS concentration on Earth [4].

In the IPB, the nature of the link between volcanism and VMS mineralization has been, and partly still remains, a matter of debate [4–6]. In any case, as VMS deposits occur within volcano-sedimentary stratigraphic successions and are commonly coeval with volcanic rocks, several major research lines have been followed to assess the links between volcanism and VMS deposition, including studies on volcanic architecture and

geochemistry (X-X). These studies are relevant to the Iberian Pyrite Belt, even more so as they are still scarce, as also are U–Pb dates.

Considering the geochemical features of the volcanic rocks related to VMS deposits, several proposals have been determined worldwide, indicating that some of these features could be used as an exploration tool, as they could discriminate between barren and “fertile” (i.e., more closely linked to VMS deposits), felsic volcanic rocks. For instance, it has been claimed that most “fertile” host types are rhyolites characterized by relatively low Ce_N/Yb_N values, and distinct, negative Eu anomalies, as well as by low Zr/Y and intermediate to high HFSE contents [7–11]. The potential use of these geochemical tools is complicated by the fact that VMS deposits formed in a number of contrasting geodynamic settings, implying very different petrogenetic models [10]. Most probably, these geochemical tools are useful in a number of VMS provinces, whereas their use in other areas, i.e., in a different geological and geodynamic setting, would be questionable. In the IPB, some of these geochemical proposals have been developed in recent times, including the use of trace elements and Nd isotopic signature of felsic rocks [12–14]. The available evidence suggests that a number of geochemical tools are useful in the IPB and deserve further research.

On the other hand, the study of volcanic architecture has received particular attention in VMS provinces [15–18]. These studies are agreed to be crucial in mineral exploration because of their importance in determining the stratigraphic successions in these areas, and, therefore, the chronological relationships between volcanism and mineralization. Beyond this point, however, studies focused on the role of (paleo)volcanological studies as markers of the geological environment in which VMS deposits formed are scarce. More often, volcanological studies conclude that volcanism related to VMS deposits was essentially submarine and developed below the wave base level, with little additional precisions [19,20].

Geological studies in the IPB have followed this general trend until very recent times. However, recent research has shown that the detailed study of the volcanic successions in this province allows to determine that volcanic successions in areas where VMS deposits occur not only emplaced below the wave base level, but in a deepwater environment, consistent with the water depth required to VMS formation [21,22]. Accordingly, the study of volcanic successions is also important as a paleoenvironmental marker in the province, and, hence, as a tool in selecting areas for mineral exploration.

The aim of this study is to show that the combined use of volcanological and geochemical tools can contribute to evaluate the potential of particular areas in the IPB province in terms of mineral exploration. We show that in the El Almendro–Villanueva de los Castillejos (EAVC) area in the Spanish IPB felsic magmatism is similar (although not identical) in petrological, geochemical, isotopic signature and U–Pb date to other felsic volcanic rocks in the IPB linked to some VMS deposits. However, volcanological study provides compelling evidence for shallow water volcanism, having produced pyroclastic, eruption-fed deposits. Such a shallow water environment precluded VMS formation.

Apart from showing the usefulness of the combined use of geochemical and volcanological tools in VMS exploration, we compare this case with others in the IPB to reaffirm that most of the VMS deposits in the province have a link with felsic volcanic rocks. Differences among the many VMS deposits in the area, however, are worth noting. They are mainly controlled by basin compartmentalization, which implied (a) the melting of different crustal segments, both in space and time, as shown by contrasting Nd signatures and U–Pb ages; (b) strong paleoenvironmental differences within the belt, including drastic changes in water depth.

2. Geological Setting

The Iberian Pyrite Belt (Figure 1) consists of three tectonostratigraphic units. From bottom to top, they are named the Phyllite–Quartzite (PQ) Group, Volcano–Sedimentary Complex (VSC) and Culm Group [23]. The basal unit is the PQ Group, consisting of quartzarenites and shales. High-energy, sedimentary deposits have been locally reported at the top of this unit [24]. A Late Famennian age is indicated by conodonts and other fossils’

occurrence for the uppermost part of the sequence [25]. The PQ Unit is exposed in the core of the two major regional antiforms in the eastern South Portuguese Zone (Figure 1). The contact between the PQ and the overlying VSC is agreed to be an essentially stratigraphic contact, though locally affected by overthrust systems.

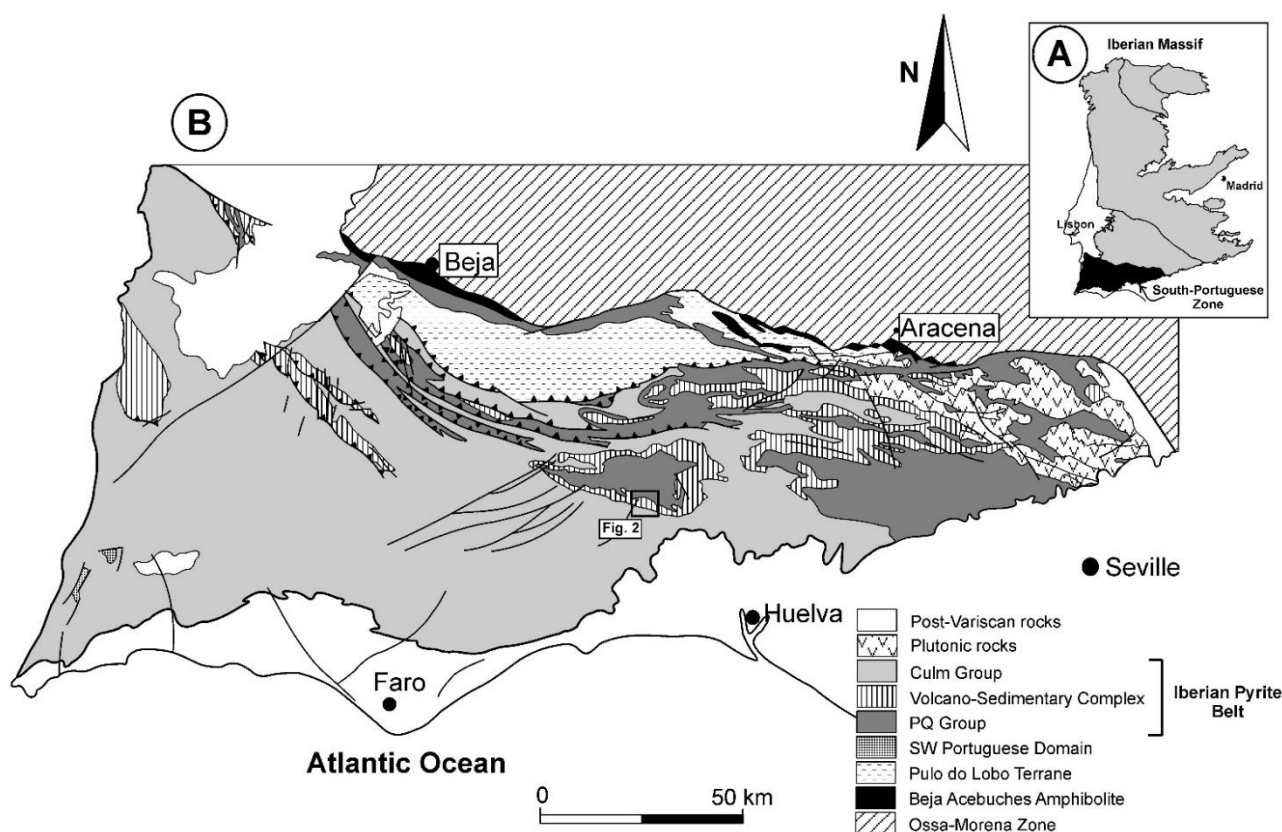


Figure 1. General map of the IPB (B). The insert (A) shows its location within the Iberian Massif in the Iberian Peninsula.

The VSC, which hosts all of the huge and numerous VMS deposits in the IPB [4], mainly consists of volcanic and subvolcanic rocks with interfingered sediments, including volcanoclastic rocks, shales and siliceous deposits (chert, jasper) located at different stratigraphic levels. Depending on zones, the relative thicknesses of volcanic piles and interfingered sediments widely vary in the IPB, implying sharp lateral changes in the sedimentary environment. In turn, this reflects a subdivision—probably of tectonic nature—of the main basin.

Volcanic rocks mainly comprise felsic and mafic volcanic and subvolcanic rocks, together with minor andesites. Mafic rocks are basaltic in composition and generally subalkaline, although minor, alkaline basaltic rocks have been described. Felsic rocks mainly comprise dacitic and rhyolitic rocks. A relative abundance of felsic and mafic rocks, as well as that of dacites and rhyolites within the felsic units, is also widely variable depending on sectors [26–31]. Again, this is considered to reflect domain division within the IPB, which remains insufficiently understood.

Given the importance of the VSC, both in theoretical and economic terms, we considered that the available dates in this unit were still insufficient. However, a number of reliable dates in the VSC rocks have been obtained in recent years, both by U–Pb and palynological methods. Regarding palynological dating, the basal part of the VSC was dated first as Late Famennian [32], whereas Moreno et al. and González et al. [24,33] have established the beginning of the volcanic activity in the area, as well as the age of several massive sulfide deposits intercalated in a sequence of black shales, which contain spores of the LN Biozone and yield a Strunian age, approximately corresponding to 362–360 Ma.

Regarding the U–Pb dating, Barrie et al. [34] focused on felsic rocks spatially related to VMS deposits, reporting that some of these volcanic rocks are older than 355 Ma, whereas in other areas volcanisms (and the presumably related VMS deposits) were younger. Both the protracted igneous activity and the diachronic character of the VMS deposits have been recently confirmed with new U–Pb dates in various areas in the Spanish IPB [12,14], depicting a time span roughly comprised between 354 and 346 Ma, both for magmatic activity and mineralization.

Although the geotectonic interpretation of the VSC is still a matter of debate, it is generally agreed to have formed in a transtensional setting, related to a global scenario of continental collision [28,35,36].

The uppermost Iberian Pyrite Belt unit is the denominated Culm Group. It consists of a thick flyschoid deposit, namely, mainly constituted by consisting of shales and greywackes. It contains goniatite and conodont fauna, yielding a Late Viséan to Namurian age [37].

3. Geology of the VSC in the EAVC Area

3.1. Structural Features

The EAVC Area is located at the SW flank of the Puebla de Guzmán Antiform (PGA), a major structure in the Southernmost Spanish IPB. Previous structural studies in this area indicate that the Southern limb of the PGA is constituted by a system of N110W thrusts in which the upper block displaced towards the SSW, implying local thrusting, both of the PQ Group over the VSC and the VSC over the Culm Group. This system of overlapping thrusts is consistent with generalized thin-skinned tectonics, in which the total shortening would be the sum of the discrete displacements of numerous faults [38,39]. In places, faulting has produced polymictic breccia packages containing abundant fragments of milky quartz, likely related to rock veining and fracturation.

A sketch map of the studied area is shown in Figure 2. Apart from the main thrusts and faults it shows, it is worth noting that other minor faults occur, a number of which within the VSC. In these circumstances, the lithological sequence in Figure 2 has a limited stratigraphic value. It is apparent, for instance, that the bottom of the VSC in the EAVC zone is not observable due to the PQ overthrust. For this same reason, the total thickness of the VSC is difficult to estimate. Possibly, it could approach 500 m at most, including its upper sedimentary package.

3.2. Petrographic and Volcanological Description: Interpretation of the VSC Volcanic Rocks

Field study shows that all of the outcropping felsic rocks correspond to two groups: a lower fiamme-rich volcanoclastic rhyolite package, and an upper coherent, quartz and K-feldspar-phyric rhyolite package. This chronological interpretation of the sequence, which is inferred from field observations, was confirmed by U–Pb dating as described below. The Upper VSC in the studied area is dominated by shales, including the purple shale horizon that marks the VSC top at a regional scale.

Although less abundant than felsic rocks, coherent mafic rocks also occur in the studied area. Considering the above described lithological succession, they locate between the volcanoclastic and the coherent felsic rocks. However, their relative chronology with regard to felsic rocks cannot be interpreted with the available evidence, as contacts between mafic rocks and their hosts appear to be intrusive in a number of instances, whereas in other cases are clearly cut by faults.

Considering first the above described mafic rocks, they are massive and coherent. They show a non-porphyrific, subophitic texture, mainly composed by augitic clinopyroxene, plagioclase and chloritized pseudomorphs, possibly corresponding to former olivine crystals (Figure 3A). Alteration minerals include albite, sericite, chlorite, and carbonates, together with minor titanite and rutile. Considering the texture and composition, they could correspond to subvolcanic intrusive bodies. A similar conclusion has been previously suggested, also highlighting the fact that no mafic fragment has been observed in the surrounding volcanoclastic or sedimentary rocks [40].

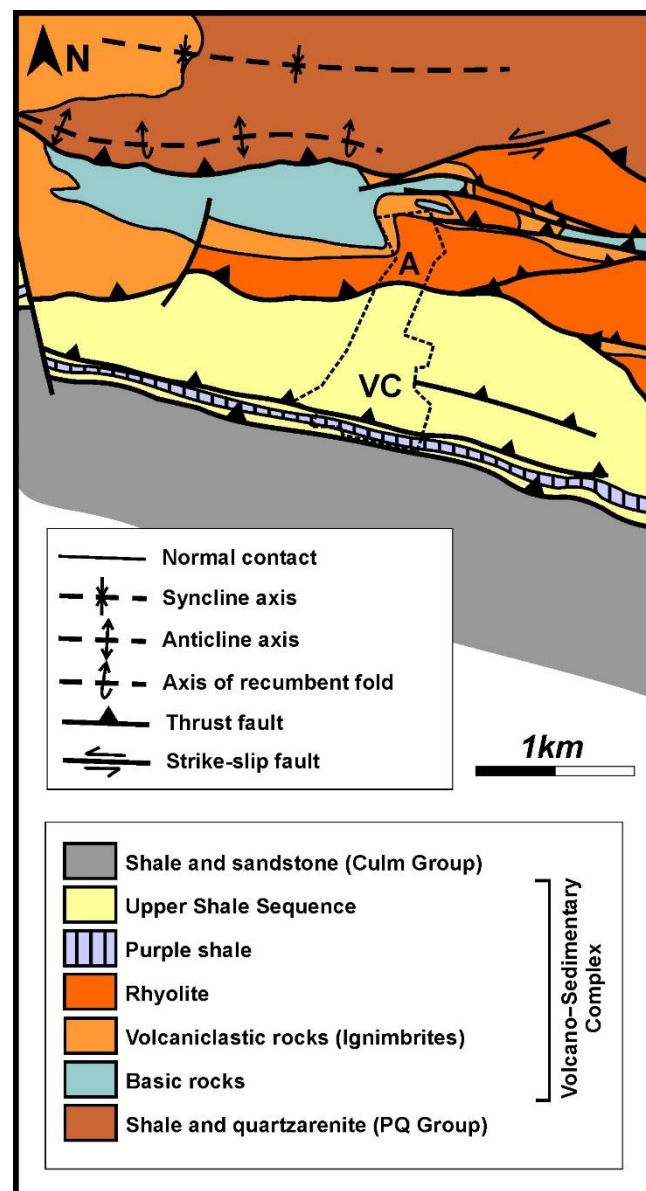


Figure 2. Sketched geological map of the studied area, showing the major thrust and fault structures. Abbreviated locality names: A, El Almendro; VC, Villanueva de los Castillejos. Modified from [39].

We, henceforth, focused on the genetic interpretation of the felsic rocks in the EAVC area and the paleogeographical evidence they provide, which is considered relevant with regard to VMS deposits. As indicated above, and in contrast with the diversity of felsic volcanic facies associations in other areas in the IPB, in the EAVC the occurring felsic rocks correspond only to two contrasting volcanic types: a lower volcaniclastic and an upper coherent facies association.

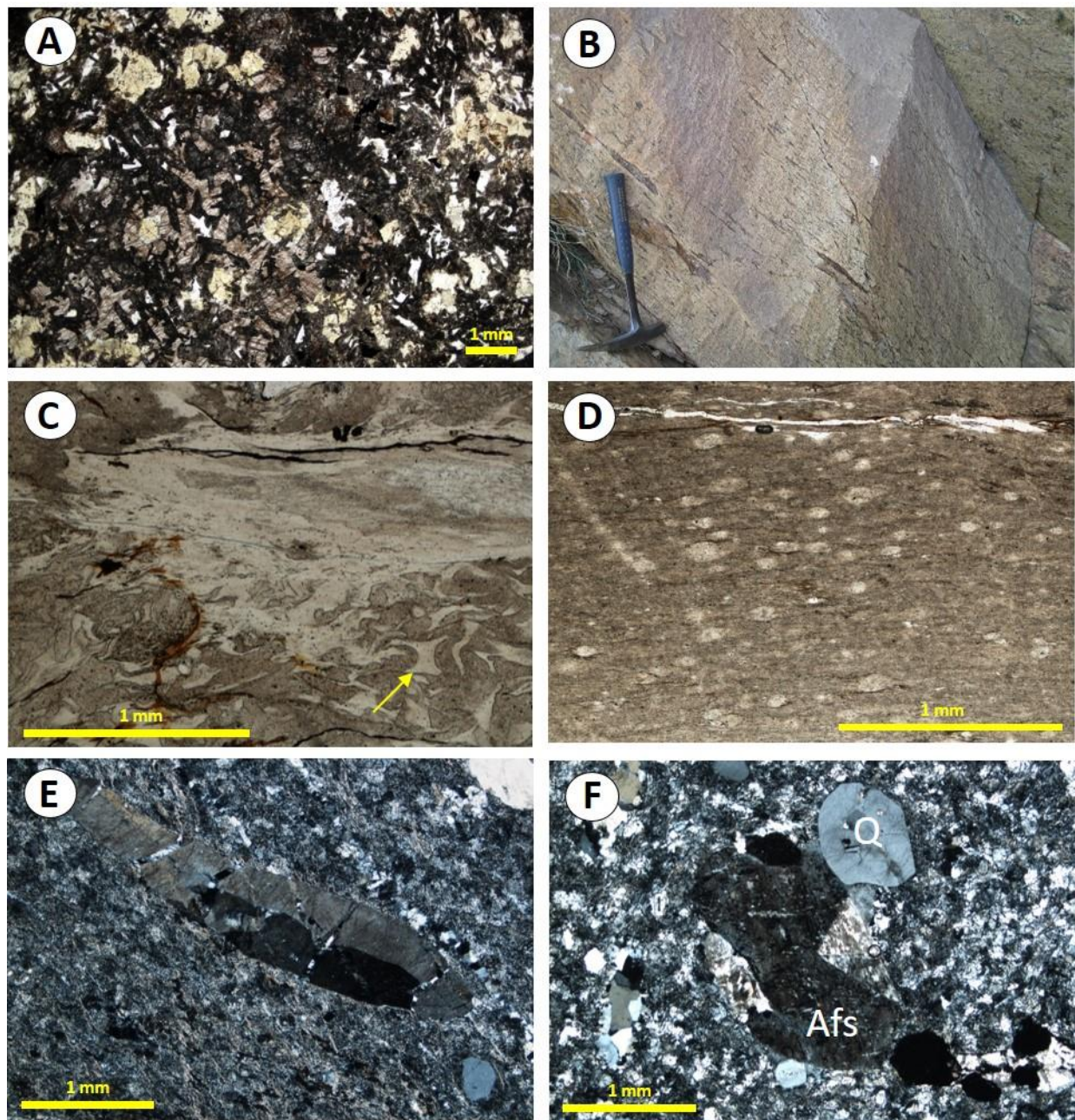


Figure 3. Field and textural features of igneous rocks in the EAVC area. (A) Texture of (probably subvolcanic) mafic rocks. Crossed polars. (B) Field view of a felsic, fiamme-rich volcaniclastic deposit. (C) Fiamme and glass shards in volcaniclastic rocks. Plane polarized light. (D) Radiolaria in a shaly horizon overlying the volcaniclastic succession. Plane polarized light. (E) Porphyritic texture in coherent rhyolites. Crossed polars. (F) Textural evidence for matrix recrystallization in coherent rhyolites; complex substitution textures in K-feldspar phenocrysts and pervasive micropoikilitic texture in the rock matrix. Crossed polars.

Regarding the felsic volcaniclastic facies association, previous descriptions have reported at least two packages in the studied area, separated by the above described mafic rocks [40–42]. Both packages consist in clast- to matrix-supported deposits, the lower one reaching up to 70 m thick. They are characterized by fiamme-like fragments, variable in size but up to 10 cm in length, parallel to the rock foliation (Figure 3B). In places, these deposits are roughly graded, with increasing grain size towards the top of the deposit [42]. Previous works subdivide the lower volcaniclastic package in three volcanic facies, only distinguished by grain size and exhibiting gradual contacts [40].

Fiamme fragments are sericitic and contain feldspar and quartz phenocrysts, which can also occur in the rock matrix as isolated crystals and fragments. The fiamme fragments are ragged in shape with wispy terminations. Their shape suggests the flattening of highly vesiculated pumiceous fragments. In most places, the matrix is mainly sericitic, together with some quartz that could be related to post-magmatic recrystallization, linked to regional alteration processes. Glass shards also occur in the matrix of the volcanoclastic rocks, showing no evidence for tectonic-related deformation (Figure 3C).

A first, early interpretation of this unit suggested that the described volcanoclastic rocks could correspond to eruption-fed pyroclastic, ignimbritic deposits, in either subaerial or shallow marine. This interpretation, however, was determined with caution for two reasons: first, the pyroclastic fiamme fragments, at least in part, could have been tectonically flattened during Variscan deformation. Additionally, real evidence for hot emplacement was considered inconclusive [41]. Even admitting that fiamme fragments are undoubtedly pyroclasts, further criticisms to an ignimbritic origin of these deposits have been exposed in detail, mainly arguing the lack of positive evidence for hot emplacement, such as perlitic matrix, columnar jointing or any other. Accordingly, a probably submarine environment, at a loosely defined depth, was proposed [40], also remarking the occurrence of marine fossils [18].

However, according to the generalized eutaxitic textures and negative grading, as well as the occurrence of glass shards in the rock matrix, we returned to interpret the fiamme-rich volcanoclastic deposits in the EAVC area as an ignimbritic deposit, in either subaerial or very shallow marine. We rather favored this latter possibility in view of the occurrence of interbedded, shaly horizons containing radiolaria towards the top of some of the described volcanoclastic packages (Figure 3D) [42]. In contrast, transport into a deepwater environment is unlikely, as the resulting deposit should exhibit much more conspicuous lamination and grading.

The upper part of the volcanic succession in the studied area is represented by rhyolitic coherent rocks, outcropping as masses up to 60 m in thickness with a maximum length of 500 m hosted by fine-grained sediments [41]. They often exhibit columnar jointing, showing variable dipping within the individual bodies. A close jointing normal to the columnar prisms is often observed, which is also probably related to magma cooling.

Coherent rhyolites are porphyritic, consisting in quartz and K-feldspar phenocrysts (Figure 3E), together with less abundant pseudomorphs of other phenocrysts that could correspond to completely altered biotite or amphibole, although relics of these minerals are absent. Vesicles are conspicuous, in places flow-flattened and filled with quartz. Some of them can reach in places up to 10 cm in equivalent diameter.

The groundmass of coherent felsic rocks is microcrystalline, essentially composed by quartz and K-feldspar in variable proportions. However, evidence for intense alteration and groundmass recrystallization is compelling. Apart from the complete substitution of mafic phenocrysts, this is also shown by the micropoikilitic texture of the matrix, quartz overgrowth rims around quartz phenocrysts and the complex substitution textures in the feldspar phenocrysts (Figure 3F). This accounts for some of the geochemical features of these rocks, as discussed below.

We interpreted that the above geometric and petrographic features could correspond to the dome-shaped emplacement of felsic, shallow subvolcanic rocks. The only possible depth constraint would be given by vesiculation, which roughly suggests a shallow environment [43]. It should be noted, however, that the most common volcanic facies associations of deepwater, dome-related rocks in the IPB include a wide variety of volcanoclastic facies, all of them linked to a magma–seawater interaction. Among others, peperites, hyaloclastites or volcanoclastic deposits related to dome collapse are very common all along the IPB [21,22,40]. To date, none of these facies have been found in the studied area [40,41].

4. Whole-Rock Geochemistry and U–Pb Dating

4.1. Analytical Methods

The chemical composition of volcanic rocks was determined at SGS Laboratories in Canada by X-ray fluorescence spectrometry (XRF) and inductively coupled plasma mass spectrometry (ICP-MS). The results are reported in Table A1.

The two types of felsic facies distinguished in the EAVC were investigated by the U–Pb zircon dating method: ISOD-11 (EAVC rhyolite) and ISOD-12 (EAVC pyroclastic breccia). Zircons were analyzed by high-precision isotope dilution thermal ionization mass spectrometry (ID-TIMS) at the Jack Satterly Geochronology Laboratory (Department of Geology, University of Toronto, Toronto, ON, Canada). U–Pb data for all samples are presented in Table A2. In these, associated ages and errors were calculated using the IsoPlot/Ex (v. 3.00) Excel Add-In [44].

Sm and Nd concentrations and $^{143}\text{Nd}/^{144}\text{Nd}$ isotope ratios were measured by ID-TIMS at Université Blaise Pascal (Clermont-Ferrand, France), using the analytical methods reported in Pin et al. [45]. Initial ϵNd values were calculated using U–Pb zircon ages obtained in this work, and are relative to a chondritic uniform reservoir (CHUR, equivalent to Bulk Earth) with the following present-day characteristics: $^{143}\text{Nd}/^{144}\text{Nd} = 0.512638$ and $^{147}\text{Sm}/^{144}\text{Nd} = 0.1966$ [46]. TDM neodymium model ages were calculated relative to a model depleted mantle described by $\epsilon\text{Nd}(T) = 0.25 T^2 - 3 T + 8.5$, where T is the age in Ga [47]. Data are given in Table A3.

4.2. Major Element Geochemistry

Apart from chemical analyses specifically performed for this study, we also used two chemical analyses of fiamme-rich pyroclastic rocks available from studies published by the Regional Government of Andalucía (Spain) [48]. Results are included in Table A1.

The list also includes the data we obtained for the basic rocks in the studied area. However, we have not displayed the data of basic rocks in the following figures for clarity, given that our work focused on the link between felsic rocks and VMS deposits. However, we did determine one exception with a diagram for rock classification based on immobile trace elements (see below), in order to show that in the studied area, as in most zones of the IPB, igneous rocks are bimodal in composition and mafic and felsic rocks are chemically unrelated [29,49].

In the IPB all the volcanic and subvolcanic rocks were altered at a regional scale, so that igneous rocks have not preserved their original, igneous composition. Alteration is generally ascribed to seafloor hydrothermal circulation at a regional scale, and has been named regional alteration [50]. In the vicinity of IPB deposits, haloes of focused, more intense chloritic and sericitic alteration developed over regionally altered rocks.

Although in general regional alteration is most often weak to moderate, as shown by the preservation of delicate igneous textures in many points, it is intense and pervasive enough to modify the chemical composition of rocks, especially changing the abundance of mobile elements. For this reason, major element geochemistry provides limited information on rock petrogenesis and evolution, except regarding the alteration processes themselves. This was the case in the studied area, in which we found, in addition, that both volcanoclastic and coherent rocks have experienced contrasting alteration.

The K_2O vs. SiO_2 diagram (Figure 4A) reveals these differences. Most of the analyzed rocks, both volcanoclastic and coherent, showed very high SiO_2 contents (even up to 80 wt%), which can be explained in terms of silicification related to regional alteration. This silicification is relatively common in other areas in the IPB.

In contrast, coherent and volcanoclastic rocks in the EAVC sector showed very different K_2O contents; whereas felsic volcanoclastic rocks showed relatively low K_2O contents, this is much higher in coherent rocks. Among these, only some showed contents slightly higher than those in the volcanoclastic rocks, whereas many of them showed K_2O contents ranging from 6 to 8 wt%.

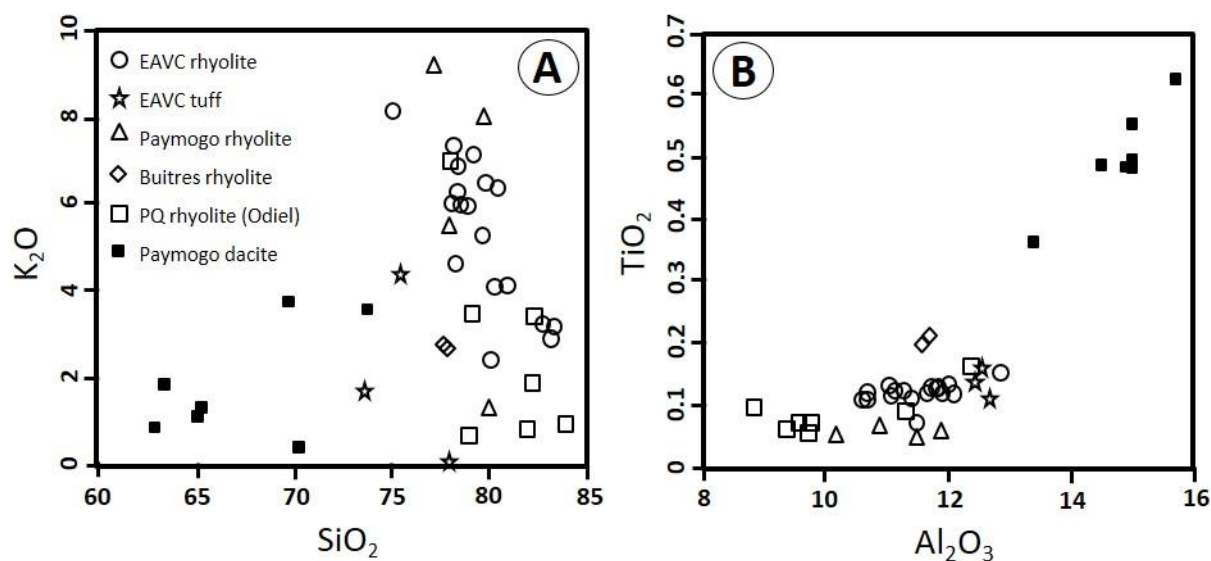


Figure 4. (A) K_2O vs. SiO_2 variation diagram. (B) TiO_2 vs. Al_2O_3 variation diagram. The chemical compositions of other groups of felsic rocks in the Spanish IPB are included for comparison.

These contents cannot be easily explained as related to a peculiar, K-rich magma type; considering the diagram based on the relatively immobile major elements TiO_2 and Al_2O_3 , both volcanoclastic and coherent rocks were plotted within a relatively narrow, overlapping variation range (Figure 4B). On the other hand, invoking the occurrence of a particular, high-K (or even shoshonitic) magmatism in this area had to be discarded, also in view of the rest of the available geochemical evidence as discussed below. Therefore, we conclude that postmagmatic, potassic alteration characterizes the coherent felsic rocks in the studied area. We also note that, whereas silicification is an almost ubiquitous, common alteration process in the IPB, intense potassic alteration is much rarer [14].

4.3. Trace Element Geochemistry

Given the pervasive alteration observed in all of the igneous rocks in the studied area, rock geochemical classification is presented first based on trace immobile elements according to the proposal by Winchester and Floyd [51]. Accordingly, volcanoclastic and coherent felsic rocks are plotted in Figure 5, together with mafic rocks in order to show that volcanism is bimodal and basic and felsic rocks are chemically unrelated, as it generally is in the IPB.

Apart from showing that both volcanoclastic and coherent rocks have a rhyodacitic composition with a narrow variation range of their Zr/TiO_2 and Nb/Y ratios, the diagram also shows that the studied felsic rocks do not show substantial differences with regard to rhyolitic felsic rocks analyzed in other areas within the IPB, in which geochemistry, Nd signature and age are well known [12,14].

The close geochemical similarity between the studied volcanoclastic and coherent rocks, as well as that observed between these groups and other felsic rocks in the Spanish IPB, was confirmed by plotting the primitive mantle-normalized contents of incompatible trace elements of all the rocks on spider diagrams (Figure 6), as well as by the display of their chondrite-normalized REE spectra (Figure 7). It is also apparent that the studied rocks are closely similar to other groups of felsic groups that are spatially related to VMS deposits, such as those in the upper part of the Riotinto–Nerva Unit [12] and those in the Paymogo area [14].

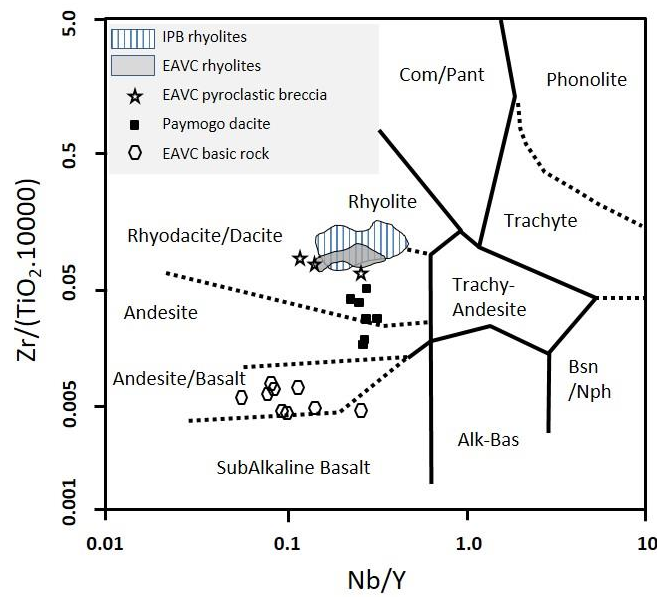


Figure 5. Classification of the felsic and mafic rocks in the EAVC area according to the proposal by Winchester and Floyd [51]. Data of “IPB rhyolites” were taken from [12,14]. “Paymogo Dacite” samples were taken from [14].

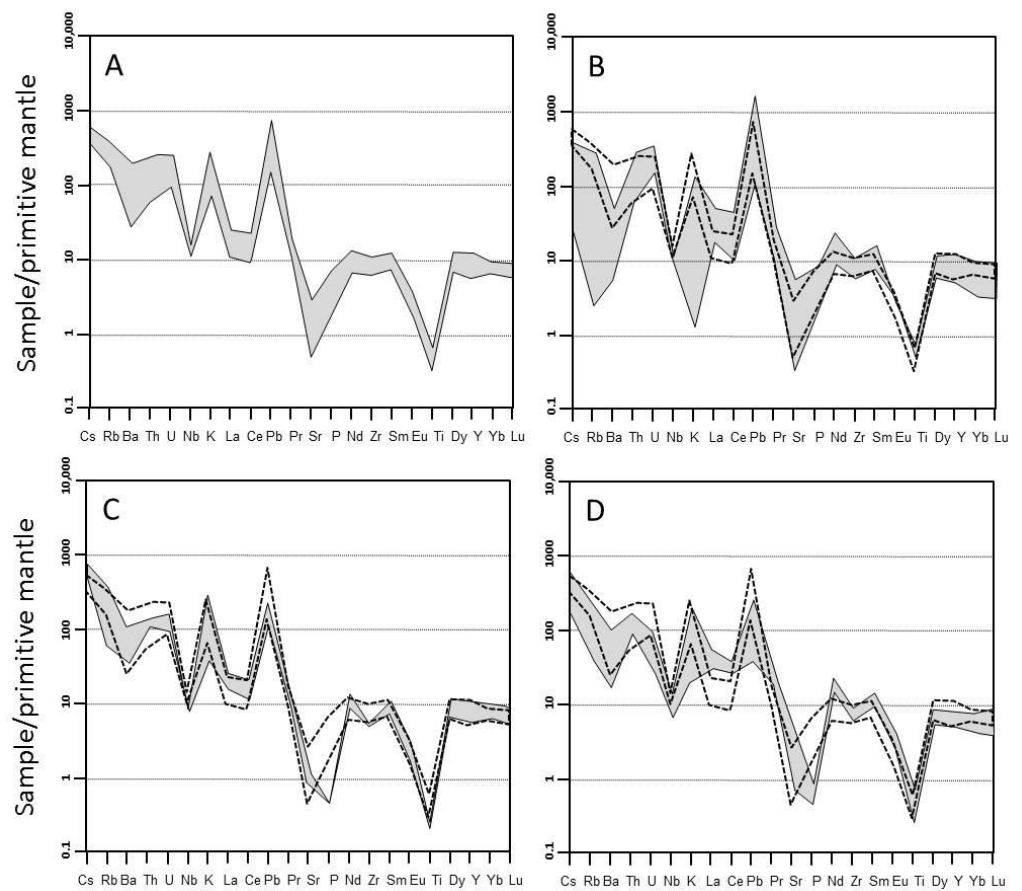


Figure 6. Spectra of incompatible elements normalized to primitive mantle [52] for the felsic rocks in the EAVC area and other felsic rocks in the Spanish IPB. (A) EAVC rhyolite. (B) EAVC pyroclastic breccia. (C) Paymogo rhyolites [14]. (D) Rhyolitic rocks in the upper sequence of the Odiel area [12]. The area limited by a dashed contour line in (B–D) corresponds to the variation range of the EAVC coherent rhyolites as displayed in Figure 6A.

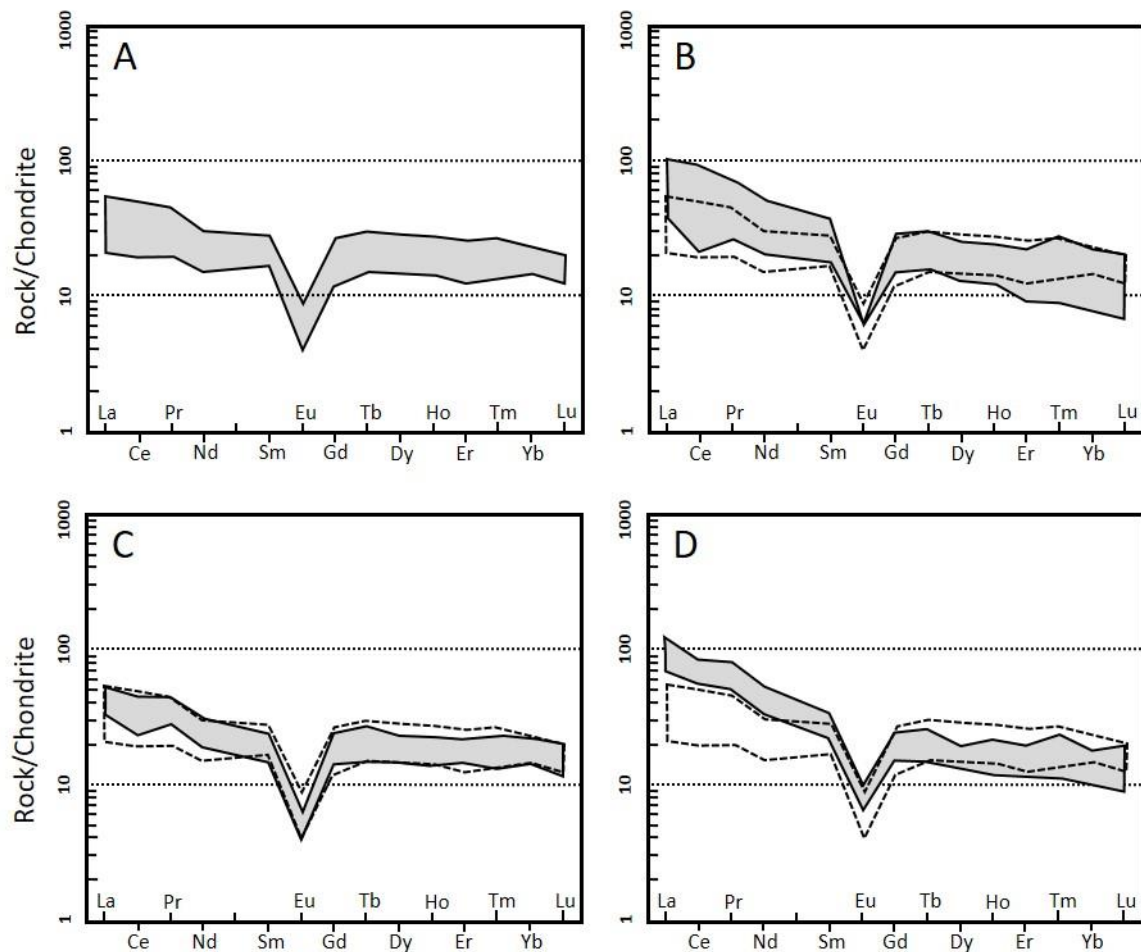


Figure 7. Chondrite-normalized REE diagrams [53] for the felsic rocks in the EAVC area and other felsic rocks in the Spanish IPB. (A) EAVC rhyolite. (B) EAVC pyroclastic breccia. (C) Paymogo rhyolites [14]. (D) Rhyolitic rocks in the upper sequence of the Odiel area [12]. The area limited by a dashed contour line in (B–D) corresponds to the variation range of the EAVC coherent rhyolites as displayed in Figure 7A.

Primitive mantle-normalized diagrams show the close chemical composition of coherent and volcanoclastic rocks with the obvious exceptions of K, Rb and Ba, all of them related to potassic alteration of coherent rocks (Figure 6A,B). Apart from this, the only minor difference between both groups was the lesser P content in some (not all) of the volcanoclastic rocks. Regarding other felsic rocks in the Spanish IPB, the similarity between felsic rocks in the studied area and those in the Paymogo sector [14] was almost complete (Figure 6A,B,D). It is worth to note that, in the Paymogo area, potassic alteration has also been reported [14].

Chemical similarities, both between the two groups of felsic rocks we have distinguished in the EAVC and with regard to other felsic rocks in the Spanish IPB, were also obvious in chondrite-normalized, REE diagrams. Comparing volcanoclastic and coherent felsic rocks in the studied area, both groups share a similar Eu anomaly, as well as flat HREE spectra with an overlapping range of Tb_N/Yb_N ratios (Figure 7A,B). Some of the volcanoclastic rocks show slightly higher LREE contents and a slightly higher La_N/Sm_N ratios. Again, the REE spectra of the studied rocks were very similar to those in other felsic rocks in the IPB. In particular, the felsic rocks in the EAVC zone and the Paymogo rhyolites [14] showed almost identical REE patterns (Figure 7A,B,D). In all cases, the flat HREE pattern of felsic rocks indicates that the source area of felsic magmas was not in equilibrium with garnet.

4.4. Nd Isotope Geochemistry

Although only a limited Nd isotope dataset was available, these data indicated that the felsic rocks in the area under study were generated from an evolved, crustal source ($-4.7 < \epsilon\text{Nd} < -4.5$). In addition, a comparison between chemical and isotopic results in the EAVC zone and those obtained in other areas of the Spanish VSC showed that these values also occurred in other areas in the IPB such as the Paymogo Volcanic Sedimentary Alignment (PVSA), where felsic rocks, generated from evolved crustal segments, are related to VMS deposits [14]. This comparison, however, is not strict because, in this latter area, the felsic volcanic rocks showed a wider range of Nd values, comprised between -5.3 and -4.1 for the highly evolved dacites and rhyolites, and between -3.2 and -2.9 for the Paymogo rhyolites. In any case, the above ϵNd values were in all cases consistent with the generation of felsic magmas from the evolved crustal areas.

4.5. U–Pb Dating

Two U–Pb age determinations were performed in the EAVC area. They, respectively correspond to a pyroclastic (sample ISOD-12) and a coherent felsic rock (sample ISOD-11). Results are plotted on a Concordia diagram in Figure 8.

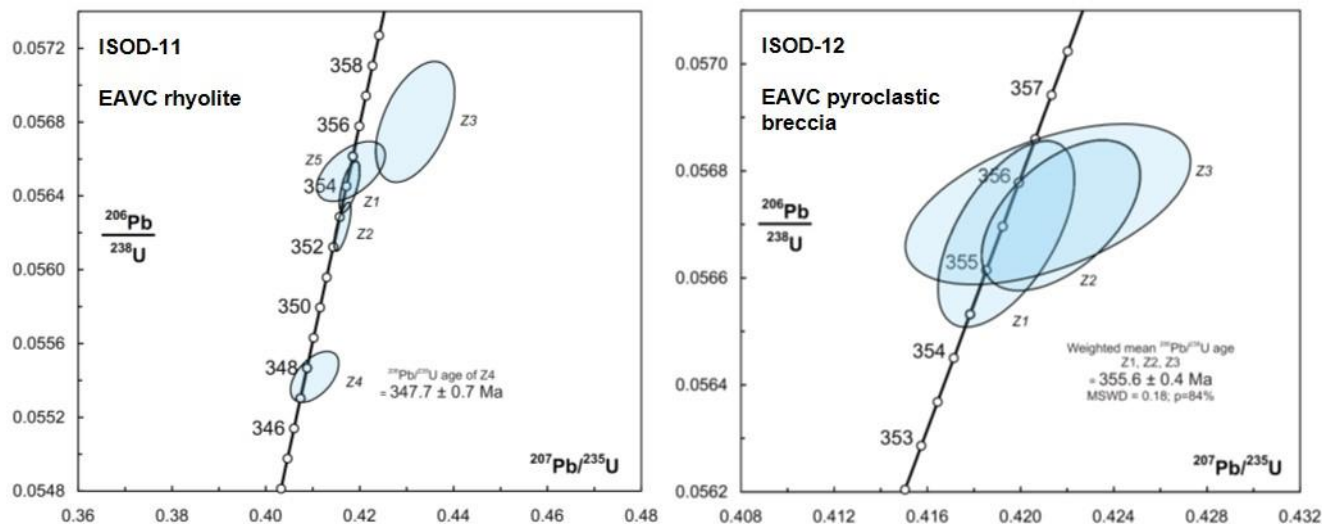


Figure 8. U–Pb Concordia diagrams for zircon grains obtained from pyroclastic breccia and rhyolite samples in the EAVC area. Ages based on single sample or mean $^{206}\text{Pb}/^{238}\text{U}$ ratios. Error ellipses in the Concordia diagrams are shown at the 2σ level.

The obtained U–Pb ages indicated the time interval for the EAVC felsic volcanism, comprised between the 355.6 ± 0.6 Ma of the age of the analyzed felsic volcanoclastic rock and the 347.7 ± 0.7 Ma obtained for the dated coherent rhyolite/rhyodacite. This interval suggests a relatively long-lived volcanic activity, as it is the case in other areas in the IPB. For instance, U–Pb dates in the Riotinto–Nerva Unit shared a volcanic time span similar to that of the studied area [12]. On the other hand, geological evidence strongly suggests that the VSC must have covered a much larger interval, in view of the thickness and petrological complexities of the volcanic successions in the region [14,28–30].

Nevertheless, the 347.7 ± 0.7 Ma “age” for coherent rhyolites (sample ISOD-11 in Figure 8) relies on the age obtained from a single zircon grain (Z4): the rest of the analyzed zircon grains in ISOD-11 delimited an age cluster that overlapped with that of the analyzed zircons in the EAVC pyroclastic rock ISOD-12, suggesting that the two analyzed rocks emplaced at very close ages. Actually, recalculating the age of ISOD-11 after excluding Z4 would lead to a weighted average of 354.2 Ma. That would make it only slightly younger than the pyroclastic breccia ISOD-12. Regarding the analyzed Z4 zircon, its “age” could well be a reflection of Pb-loss. We proposed to adopt this latter alternative. Accordingly,

we interpreted that both coherent and pyroclastic rhyolites in the EAVC emplaced within a time interval of less than 1 Ma.

Apart from the fact that this interpretation is more consistent with the whole of U–Pb ages obtained both in the ISOD-11 and ISOD-12 samples, it also leads to a more coherent geological interpretation at a regional scale. In all the IPB areas hosting VMS deposits in which combined geochemical study and U–Pb dating were performed, wider time spans of felsic volcanic activity involved significant geochemical changes [14,28–30]. Accepting a wide interval for the EAVC volcanism would imply that the EAVC area would be the only case in the IPB in which protracted volcanic activity would have occurred without significant geochemical or isotopic changes. This would be a rare circumstance at a regional scale.

5. Discussion

The EAVC succession did not substantially differ from others in the VSC. It represents a relatively complete VSC sequence in which its upper and lower limits can be recognized. Its total estimated thickness was lower than in the Riotinto–Nerva Unit [21], but felsic rocks are as well represented as in many other VSC successions. The petrographic, geochemical and isotopic features were roughly similar to those in other felsic rocks elsewhere in the IPB [12,14]. Regarding the relative abundance of interbedded sediments, the VSC in the EAVC section contained more sediments towards the top, for instance, than the Riotinto–Nerva Unit; but sediments were not as abundant as in relatively close areas, including the Northern branch of the Puebla de Guzmán Antiform (PGA), where the VSC sequence is dominated by sediments in many points [54].

In spite of the above quoted similarities, the most striking feature of the VSC not only in the EAVC area, but in all the Southern branch of the PGA, is that VMS deposits have not even been reported in this area, where only scarce, small manganese deposits are cited [4]. In contrast, VMS deposits were abundant in the Northern branch of the PGA, including the Tharsis supergiant deposit [4].

5.1. Geochemical Features and Nd Signatures of the EAVC Felsic Rocks

As in most of the IPB areas, the felsic rocks in the EAVC area are related to the melting of more or less evolved crustal segments [12,14]. The low Tb_N/Yb_N ratios in felsic rocks indicate that they did not form in equilibrium with a garnet-bearing source at maximum estimated depths of 30 km [10]. The interpretation that crustal melting affected to evolved, relatively shallow crustal segments was consistent with the negative ϵNd signature of felsic rocks. In all, these features suggest progressively crustal melting related to transtensive geodynamic environment [12], probably related to basic magma underplating [55].

The available geochemical features of the EAVC showed little or no geochemical differences between volcanoclastic and coherent rocks: the only immobile major elements, Al and Ti, the distribution of trace incompatible elements and the REE spectra, displayed closely similar values. Importantly, they are all classified as chemically similar rhyodacites in diagrams based on immobile trace elements because they have similar Ti/Zr ratios. Moreover, ϵNd signatures of volcanoclastic and coherent rocks were also similar. The only significant, chemical differences between the two groups were related to the intense potassic alteration shown by many coherent rocks, which are strongly enriched in K₂O, Rb and Ba. Accordingly, both geochemical features and ϵNd signature suggest that all the felsic rocks could have generated from a same evolved crustal zone.

Considering the available criteria that were previously suggested in order to discriminate between “fertile” and barren rocks in VMS worldwide, the EAVC data confirm again that previous proposals based on REE geochemistry [10] are not useful in the IPB because most of the IPB rocks, also in the studied area, plot altogether within a single field in the discrimination diagram. In order to evaluate other alternative proposals [12,13,22], we compared the geochemical features of the rocks under study with that in other sectors in the Spanish IPB. A rough chemical similarity exists between the EAVC felsic rocks and

the older felsic rocks from the PVSA area in the Northern IPB, including negative ϵNd signatures [22].

This comparison, however, is not strictly pertinent. For instance, the younger felsic sequence in the PVSA area, which are spatially related to numerous VMS deposits, were not equivalent to those in the EAVC [14]: these fertile rocks, probably representing the main VMS-related volcanic event in the PVSA and Riotinto areas [12,14], showed a distinctly different ϵNd signature with regard to the EAVC area (Figure 9).

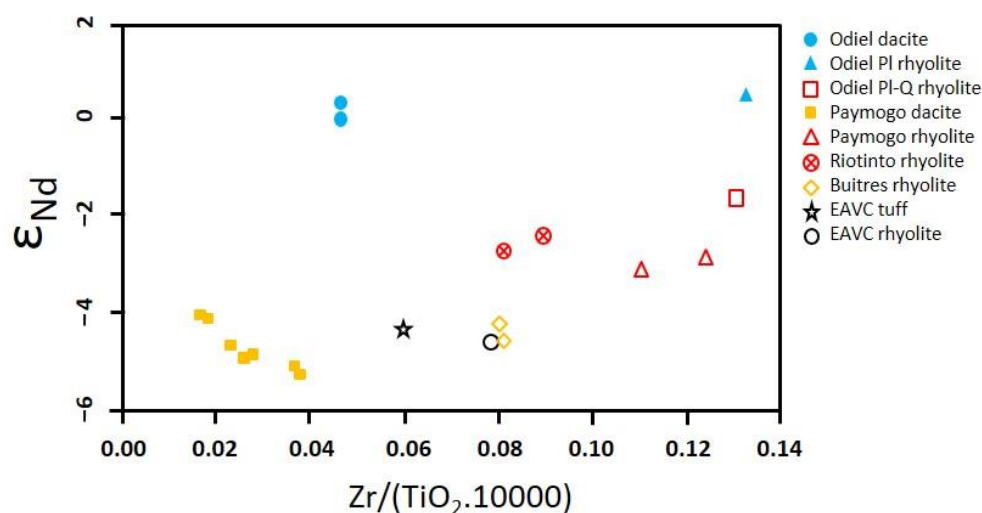


Figure 9. ϵNd vs. $\text{Zr}/(\text{TiO}_2 \cdot 10000)$ diagram of felsic rocks in the EAVC area and other felsic rocks from the IPB. Red symbols: felsic rocks linked to VMS deposits. Orange symbols: felsic rocks only locally related to small-sized VMS. Blue symbols: barren felsic rocks. Black symbols: this study.

Nevertheless, the use of the geochemical and isotopic tools proposed in other IPB areas could indicate a possible link between felsic rocks and VMS mineralization in the studied area. This is because some minor rhyolitic rocks in the PVSA, sharing the same ϵNd signature as those in the studied area, are also linked to small VMS deposits.

We conclude that the ϵNd signature was useful in indicating that the EAVC area was not linked to the main volcanic event related to VMS deposits such as those in the Rio Tinto Mining District and in the PVSA. However, at the same time, the use of this isotopic tool could suggest not to completely discard a possible connection between the felsic rocks in the EAVC and a few small VMS deposits, as some of those occurring in the PVSA [14].

5.2. The EAVC Volcanic Architecture and U–Pb Dating

A first difference between felsic rocks in the EAVC and those most commonly found in other areas in the IPB was that, in the EAVC, the felsic rocks corresponded only to two major volcanic facies: a lower volcanoclastic facies and an upper coherent facies.

As previously described, volcanoclastic rocks in the EAVC are better interpreted as ignimbrites due to their generalized eutaxitic textures and negative grading, as well as the occurrence of glass shards in the rock matrix. Most probably, they were emplaced in a very shallow marine environment, whereas post-depositional transport was unlikely because the resulting deposit should have shown conspicuous lamination and grading. Accordingly, this shallow water environment is not consistent with VMS formation.

In contrast, the felsic coherent rocks constituting the upper part of the EAVC volcanic succession provided no direct evidence regarding their emplacement. Vesiculation and sparse phenocryst content suggest a shallow emplacement with no additional precision.

It should be remembered, however, that deepwater felsic domes (or cryptodomes) in the IPB are systematically associated to a wide variety of volcanoclastic facies related to a magma–seawater (or magma–unconsolidated sediment) interaction. Depending on areas, these facies comprise peperites, hyaloclastites or volcanoclastic deposits related

to dome collapse [21,22,41,56–58]. Some of them are diagnostic of relatively deepwater emplacement, including a low aspect ratio, rhyolitic lavas, low-explosivity, deepwater pyroclastic rhyolites [21] or volcanoclastic deposits produced by the collapse of deepwater domes [22]. Contrarily, none of these volcanoclastic facies have been described to date in the studied area [40–42]. Consequently, a comparison between the volcanic facies in the studied area and in other IPB areas in which volcanism occurs at deeper environments is shown in Figure 10.

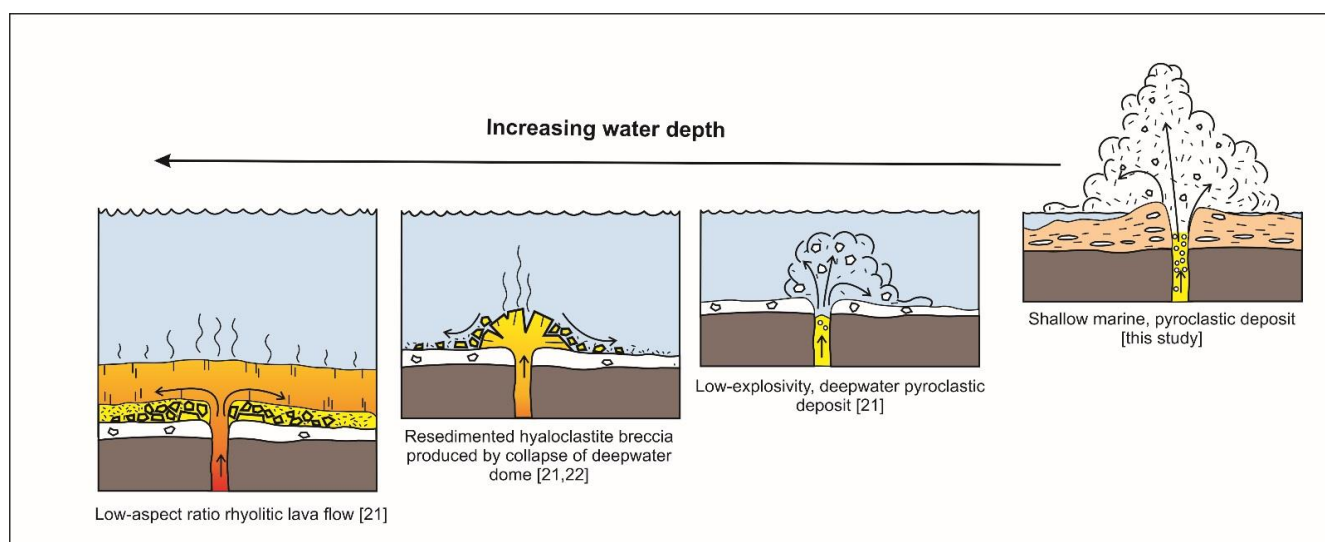


Figure 10. Comparison of the shallow eruptive environment of the pyroclastic felsic rocks in the EAVC with deeper volcanic environments of felsic rocks in other areas in the Spanish IPB.

Accordingly, we conclude that the most likely scenario in the EAVC consists in the deposition of ignimbritic felsic rocks in a shallow water environment, closely followed by the emplacement of dome-shaped, shallow subvolcanic rocks. We also conclude that a water/sediment–magma interaction was very limited, indicating a largely dominant shallow paleoenvironment all along a short-lived volcanic episode. These volcanological features can account for the lack of VMS in this sector of the IPB.

Apart from the volcanological evidence, the narrow time span of the felsic volcanism we interpreted in the EAVC, most likely covering less than 1 Ma, can account in itself for the lack of VMS deposits in this area; it is generally admitted that VMS formation must be related to long-lived, robust hydrothermal systems [59,60]. Therefore, it is in most of the VMS deposits in the IPB, where U–Pb dating shows a link between VMS deposits and protracted volcanic activity, along time intervals up to 6 Ma [12]. Conversely, VMS deposits are unlikely to develop if related to episodic volcanic activity, such as that in the EAVC.

5.3. Basin Compartmentalization of the IPB

For general geological reasons, it is a fact that the petrological, geochemical and volcanological study of igneous rocks is relevant in the IPB; petrology remains a major tool in defining the general environment in which the IPB basin generated and evolved, as well as in geodynamic reconstructions. Moreover, both volcanic architecture and geochemistry are crucial in establishing reliable stratigraphic successions.

However, beyond this general importance, what we showed in the EAVC is that Petrology, Geochemistry and Physical Volcanology, as previously suggested in other sectors of the IPB, are tools that can be directly used in VMS exploration, as they allow to distinguish between felsic igneous rocks that are linked (or unrelated) to mineral deposits. For instance, in other areas in the IPB, where most of the succession of felsic volcanic rocks formed in a deepwater environment [21,22], volcanologic study cannot discriminate between groups

of felsic rocks; but geochemical evidence, and in particular the ϵNd signature, can help in discriminating “fertile” and barren rocks. This is shown by the close link between felsic rocks with a given, negative ϵNd signature and VMS deposits in a number of areas in the IPB, including Rio Tinto [12,14].

The EAVC represents a different case: here geochemical evidence, including the strong negative ϵNd signature of the studied felsic rocks, indicated that the geochemical and isotopic signature of the whole sequence was consistent with crustal melting in conditions similar to that in other IPB areas, where some VMS deposits occur. In this case, however, what suggested discarding the area was the lack of evidence for a deepwater environment, which precluded VMS deposition. This interpretation was consistent with the absence of VMS all along this sector in the IPB [4]. Moreover, the narrow time span of volcanism would have not been favorable to the triggering of robust, long-lived hydrothermal systems.

We therefore conclude that in a large, complex area, such as the IPB, both geochemical and (paleo)volcanological tools were useful in mining exploration; however, the diversity of possible scenarios that may account for the interpretation of magmatism and mineral deposits all along the province indicated that they should not be used separately. Additionally, the EAVC represents a case in which felsic volcanic activity developed within a much narrower time span with regard to other IPB areas in which VMS deposits occur [12–14], highlighting so the need for further U–Pb dating in this region. Not only in order to assess the chronology of the VMS deposits and their hosts, but also as a tool in selecting areas favorable to the development of long-lived systems of hydrothermal circulation.

The diversity of geological scenarios must be interpreted in terms of basin compartmentalization, as previously suggested [50]. The study of the EAVC provided further support to this interpretation, as shown by the contrasting paleogeographic environment between this and the neighboring areas. Whereas the EAVC was characterized by shallow water, relatively abundant volcanic rocks, the close VSC areas in the Northern flank of the PGA were characterized by older thick sedimentary successions, in which volcanic rocks were not so abundant. These sedimentary sequences included Strunian black shales, linked to VMS deposits such as Tharsis.

The geometry of this basin compartmentalization, and therefore that of the different sedimentary sub-basins, remains poorly understood. Therefore, it is also the case regarding the regional geometric distribution between contrasting geochemical, isotopic signatures and U–Pb dates of each of the groups of igneous rocks in the IPB. Meanwhile, we confirmed the usefulness of the above criteria in the VMS exploration.

6. Conclusions

The petrologic, geochemical, volcanological and U–Pb study of the felsic volcanic rocks in the EAVC area, Southwestern Spanish IPB, was presented in order to evaluate the usefulness of these petrologic tools in VMS exploration. More specifically, the study showed that the evidence we provided can account for the lack of VMS deposits all along the studied area, in spite of the fact that these deposits occur in neighboring zones.

The felsic rocks in the EAVC area showed petrologic, geochemical and isotopic features similar to rocks that are linked to some small VMS deposits elsewhere in the IPB. In this case, however, any link to VMS deposits was to be discarded, as felsic rocks formed in a shallow water environment are not consistent with VMS formation.

However, we did not conclude that geochemical evidence, including the Nd signature of the felsic rocks, could not be valid in the IPB as a proxy of VMS deposits; what we suggested is that both volcanological and geochemical tools should be combined in mining exploration.

The narrow time span of the felsic volcanism in the EAVC area, probably less than 1Ma, was probably an additional factor that conditioned the lack of VMS deposits in the area, as protracted volcanic activity contributes to the installation of robust, long-lived hydrothermal systems. Consequently, we contend that U–Pb dating is also an important tool in mining exploration in the IPB.

Our study shows how unproductive areas in the IPB are close to other sectors in which even super-giant VMS deposits occur. This lends additional support to previous suggestions highlighting the importance of basin compartmentalization in this region. Compartmentalization accounts for the diversity of scenarios in which VMS deposits generated all along the IPB.

Author Contributions: Conceptualization, E.P., T.D., M.T. and G.M.; methodology, E.P., T.D., C.P. and M.A.H.; validation, all; formal analysis, all; investigation, all; resources, all; data curation, T.D.; writing—original draft preparation, E.P., T.D. and M.T.; writing—review and editing, E.P., T.D. and M.T.; visualization, T.D.; supervision, E.P.; project administration, E.P.; funding acquisition, E.P. All authors have read and agreed to the published version of the manuscript.

Funding: This research is supported by the research project “Caracterización y datación isotópicas de rocas ígneas y sistemas hidrotermales en la Faja Pirítica Ibérica Española” (BTE2003-04354, Plan Nacional I+D).

Acknowledgments: Careful revisions by anonymous reviewers have importantly contributed to improve this work and are acknowledged with thanks.

Conflicts of Interest: The authors declare no conflict of interest.

Appendix A

Table A1. Major and trace elements analyses of igneous rocks from the EAVC area.

Sample	Pyrocl. brec. CIA	Pyrocl. brec. CIA	Pyrocl. brec. CIA	Basic rock	Rhyol.																																
CV-647	CV-662	ISOD-12	AQ-H	AQ-J	AQ-N	AQ-O	AQ-R	AQ-V	AQ-W	AQ-X	AQ-Y	AQ-ZI	AQ-A	AQ-B	AQ-C	AQ-D	AQ-E	AQ-F	AQ-G	AQ-I	AQ-K	AQ-L	AQ-M	AQ-P	AQ-Q	AQ-S	AQ-T	AQ-U	AQ-Z	AQ-LL							
Major elements (%)																																					
SiO ₂	78.01	73.64	75.50	47.07	48.65	47.23	48.86	49.39	47.18	47.22	46.01	47.45	46.41	81.00	78.77	79.69	83.46	83.18	79.90	78.17	78.88	82.78	78.12	78.40	75.09	80.37	78.54	80.48	79.26	80.11	78.39						
TiO ₂	0.16	0.14	0.11	1.92	1.83	1.63	1.84	1.57	1.76	1.53	1.33	1.70	1.23	0.07	0.13	0.13	0.11	0.12	0.11	0.13	0.13	0.12	0.13	0.12	0.15	0.12	0.13	0.12	0.12	0.12	0.12	0.12	0.12	0.12	0.12	0.12	0.12
Al ₂ O ₃	12.56	12.43	12.70	16.66	16.02	16.89	15.66	17.04	14.57	16.08	16.43	15.22	17.32	11.51	12.04	11.77	10.69	11.08	11.44	12.03	12.04	11.17	11.89	11.68	12.86	11.32	11.06	10.71	11.09	12.09	11.99						
Fe ₂ O _{3t}	1.30	1.98	1.97	10.71	10.85	10.59	10.90	9.66	12.75	11.06	11.76	12.17	9.72	0.67	1.04	0.97	0.51	0.34	0.48	0.69	0.66	0.54	1.01	1.23	1.58	1.08	1.62	0.63	0.84	0.70	0.87						
MnO	0.03	0.06	-0.01	0.18	0.22	0.17	0.19	0.15	0.22	0.19	0.18	0.21	0.15	-0.01	-0.01	-0.01	-0.01	-0.01	-0.01	-0.01	-0.01	-0.01	0.06	0.01	-0.01	0.04	-0.01	-0.01	-0.01	-0.01	0.02						
MgO	0.48	0.75	0.83	7.03	5.60	7.73	6.16	6.53	8.40	7.87	7.55	7.91	9.20	0.68	0.27	0.25	0.34	0.20	0.20	0.29	0.25	0.27	0.21	0.19	0.35	0.30	0.24	0.22	0.29	0.33	0.26						
CaO	0.17	0.89	0.06	9.52	8.29	9.12	9.20	7.88	9.71	10.84	8.93	10.38	8.93	0.05	0.15	0.06	0.02	0.02	0.11	0.03	0.10	-0.01	0.18	0.20	0.28	0.12	0.19	0.02	0.14	0.14	0.18						
Na ₂ O	6.76	4.84	-0.02	3.12	4.68	3.25	3.69	4.07	2.44	2.29	3.73	2.54	3.35	0.25	0.70	0.53	0.13	0.24	0.81	0.57	0.69	0.13	1.27	2.46	0.40	1.26	0.55	0.36	0.36	2.66							
K ₂ O	0.04	1.64	4.27	0.73	0.40	0.80	0.48	0.90	0.21	0.40	0.06	0.35	0.28	4.09	5.93	5.24	3.14	2.86	6.44	7.31	5.92	3.20	5.98	4.58	8.14	4.07	6.85	6.34	7.13	2.38							
P ₂ O ₅	0.04	0.18	0.14	0.17	0.19	0.17	0.18	0.17	0.16	0.13	0.13	0.16	0.14	0.05	0.13	0.06	0.05	0.09	0.12	0.05	0.08	0.09	0.13	0.16	0.11	0.13	0.05	0.14	0.13	0.15							
LOI	0.85	2.01	2.58	2.95	3.55	2.65	2.25	2.85	2.10	2.25	3.70	2.05	3.90	1.65	0.95	1.40	1.65	1.95	0.46	0.85	1.30	1.80	1.10	0.70	1.10	1.30	0.65	1.05	0.70	1.35	1.05						
Sum	100.40	98.56	98.13	100.06	100.28	100.23	99.41	100.21	99.50	99.86	99.81	100.14	100.63	100.01	100.10	100.09	100.09	100.07	100.06	100.11	100.04	100.08	100.01	99.75	100.12	100.04	100.00	99.97	100.06	100.00	99.98						
Trace element (ppm)																																					
Rb	1.5	122	197	30	9	34	11	29	7	9	2	13	7	144	220	211	150	133	199	205	187	144	231	161	186	148	252	202	246	121	227						
Sr	117	31.7	7.1	211	330	199	179	251	126	150	171	150	180	10.6	41.6	25.3	25.6	61.8	50.7	32.3	38.4	28	36.4	39	22.5	42.6	37.1	44.1	38.8	48.7	41.7						
Ba	37	154	337	115	143	80	131	187	71	56	61	110	100	476	583	429	265	292	548	528	911	199	450	517	710	720	1030	1440	593	443	487						
Zr	125	99	66	135	134	142	127	129	101	82	73	92	99	70	102	96	83	98	99	109	100	85	102	100	124	89	102	96	99	98	106						
Y	56	53	22.8	36	38	36	35	34	34	30	19	31	23	32	36	36	36	49	36	53	42	50	39	40	48	32	40	27	39	50	45						
Nb	6.7	7.7	6	-2	3	3	2	4	5	3	5	3	2	8	10	10	10	8	10	10	10	8	11	10	8	9	11	9	10	10	9						
Sc	5	9	6	34.4	39	31.4	41.9	33.2	42.7	38.4	28.8	40.7	25.2	4.6	6.6	6.5	5.3	4.2	5.9	5.1	5	5.2	6.6	6.5	7.2	5.6	6.5	5.2	5.8	7.2	3.6						
V	11	9	19	257	278	212	296	235	312	278	220	301	185	4	4	4	3	3	4	4	3	4	5	5	6	4	7	5	5	6	5						
Cr	27	10	100	317	334	271	219	279	191	257	242	242	346	86	146	116	146	168	232	226	229	159	161	266	240	110	202	166	177	150	230						
Co	1.4	0.5	0.8	31	31	33	29	27	41	37	40	37	35	2	1	-1	-1	-1	-1	-1	-1	-1	2	3	-1	3	-1	-1	-1	-1	1						
Ni	-10	-10	-5	100	59	109	31	57	91	82	119	73	143	4	4	3	2	3	19	10	4	4	3	6	5	3	9	4	4	3	5						
Li	nd	nd	10	53	21	47	13	23	39	24	50	35	24	8	13	15	7	6	5	10	7	4	18	14	10	12	11	6	12	6	10						
Cu	-10	-10	12	52.3	38.7	69.1	44	31	62.5	52.2	82.1	58.4	37.1	10.8	5.9	4.7	3.2	4.6	4.1	6.8	4.5	2.9	2.6	5.2	7.2	2.9	5.3	3.9	3.5	3.4	6.1						
Hf	4.1	3.4	3	2	3	1	3	1	2	3	2	2	2	-1	-1	2	1	3	2	2	2	2	-1	1	-1	1	2	2	1	-1	-1						
Ta	0.78	0.65	0.6	-1	4	1	2	1	1	-1	-1	-1	-1	-1	-1	-1	-1	1	1	-1	-1	2	1	2	-1	-1	-1	-1	-1	-1	-1						
Pb	8	124	-5	18	13	11	11	12	12	11	18	13	14	11	23	24	17	18	19	13	18	17	20	22	31	16	30	52	22	15	26						
Th	23.7	13.4	5.6	1.8	0.5	1.9	1.5	-0.5	-0.5	-0.5	0.6	4	10.4	16.5	15.6	14	13	16.7	20.7	13.4	12.9	14.4	9.7	17.2	10.5	12.3	14	13.4	5.4	15.5							
U	7.29	6.63	3.45	2.5	1.8	-0.5	1.6	1.1	0.6	-0.5	-0.5	1	1	3.1	2.1	4.7	2.5	6.8	4.4	5.4	2.2	2.4	2.3	2.5	5.7	2.4	2.5	4.4	3.8	3.5	4.5						
La	34.9	15.5	12.6	6.7	10.4	6.6	9	9.3	7.2	6.6	7	6.7	6.8	6.9	13.7	14.9	14	13.5	13.7	14.9	15.6	13.8	16.5	13.2	17.8	13.5	14.1	12.2	14.1	14	14						
Ce	80	38.2	18.5	19.6	26.8	19.4	22.7	23.4	18.5	16.6	16.1	16.9	16.6	16.6	32.1	35.5	33.3	33	33.4	36.1	37	32.8	40.2	31.7	42.7	30.6	33.2	27.8	33.7	32.1	33						
Pr	8.18	4.26	2.96	3	3.7	3	3.2	3.4	2.7	2.4	2.2	2.6	2.4	2.2	3.8	4.3	3.9	3.9	3.9	4.2	4.4	3.9	4.8	3.7	5	3.6	3.9	3.2	3.9	3.8							
Nd	32.7	15.5	12.8	16.2	18.5	16.4	16.2	16.4	13.9	12.8	10.5	13.4	11.4	9.6	15.1	16.3	15.4	16.1	16	16	17	15.3	18.1	14.8	19.2	13.8	15.5	11.5	15.5	15.5	15.6						
Sm	7.53	5.01	3.6	5.1	5.4	4.9	4.9	4.8	4.6	3.8	2.8																										

Appendix B

Table A2. Zircon U–Pb isotopic data of representative felsic rocks from the El Almendro–Villanueva de los Castillejos area (Iberian Pyrite Belt).

Laboratory Number	Fraction	Weight (mg)	U (ppm)	Pb* (pg)	Pb _C (pg)	Th/U	Atomic Ratios						Age (Ma)						
							²⁰⁶ Pb/ ²⁰⁴ Pb	²⁰⁶ Pb/ ²³⁸ U	±2σ	²⁰⁷ Pb/ ²³⁵ U	±2σ	²⁰⁷ Pb/ ²⁰⁶ Pb	±2σ	²⁰⁶ Pb/ ²³⁸ U	±2σ	²⁰⁷ Pb/ ²³⁵ U	±2σ	²⁰⁷ Pb/ ²⁰⁶ Pb	±2σ
ISOD-11 Rhyolite (El Almendro–Villanueva de los Castillejos area) Location (7°15′45.46″ O; 37°30′46.58″ N)																			
MAH7208	Z1	1.4	183	15.3	0.26	0.55	3574	0.05645	0.00011	0.41773	0.00176	0.053668	0.000179	354.0	0.7	354.4	1.3	357.2	7.5
MAH7209	Z2	0.8	249	10.0	0.13	0.18	5233	0.05623	0.00011	0.41630	0.00145	0.053692	0.000135	352.7	0.7	353.4	1.0	358.1	5.7
MAH7210	Z3	0.8	32	2.7	0.12	3.12	830	0.05680	0.00027	0.43183	0.00684	0.055134	0.000781	356.2	1.6	364.5	4.9	417.7	31.7
MAH8011	Z4	0.4	473	10.9	0.60	0.22	1216	0.05542	0.00011	0.41039	0.00417	0.053706	0.000498	347.7	0.7	349.2	3.0	358.8	21.0
MAH8012	Z5	0.3	278	4.9	0.39	0.17	864	0.05653	0.00013	0.41808	0.00593	0.053635	0.000702	354.5	0.8	354.7	4.3	355.8	29.7
ISOD-12 Pyroclastic breccia (El Almendro–Villanueva de los Castillejos area) Location (7°16′11.53″ O; 37°30′34.09″ N)																			
MAH7174b	Z1	1.7	414	37.2	1.01	0.20	2469	0.05668	0.00014	0.41940	0.00239	0.053664	0.000252	355.4	0.9	355.6	1.7	357.0	10.6
MAH7175	Z2	0.6	419	14.2	0.50	0.11	1957	0.05672	0.00011	0.42173	0.00278	0.053928	0.000312	355.6	0.7	357.3	2.0	368.1	13.0
MAH7176	Z3	1.1	125	14.3	0.48	3.50	1051	0.05674	0.00012	0.42119	0.00500	0.053839	0.000587	355.8	0.7	356.9	3.6	364.3	24.7

Pb* is total amount (in picograms) of radiogenic Pb. Pb_C is total measured common Pb (in picograms) assuming the isotopic composition of laboratory blank: ²⁰⁶Pb/²⁰⁴Pb, 18.221; ²⁰⁷Pb/²⁰⁴Pb, 15.612; ²⁰⁸Pb/²⁰⁴Pb, 39.360 (errors of 2%). Pb/U atomic ratios were corrected for spike, fractionation, blank, and, where necessary, initial common Pb; ²⁰⁶Pb/²⁰⁴Pb was corrected for spike and fractionation. Th/U is model value calculated from radiogenic ²⁰⁸Pb/²⁰⁶Pb ratio and ²⁰⁷Pb/²⁰⁶Pb age, assuming concordance. Disc. (%) is the percent discordance for the given ²⁰⁷Pb/²⁰⁶Pb age. Uranium decay constants are from Jaffey et al. [61].

Table A3. Sm–Nd isotopic analyses of volcanic rocks from the EAVC area.

Rock Type	Location	Sample	Sm (ppm)	Nd (ppm)	¹⁴⁷ Sm/ ¹⁴⁴ Nd	¹⁴³ Nd/ ¹⁴⁴ Nd (±)(Measured)	ε _{Nd} (age)	T _{DM} (Ma)
Rhyolite	7°15′45.46″ O; 37°30′46.58″ N	ISOD-11	4.62	15.8	0.1769	0.512356 (7)	−4.6	3273
Pyroclastic breccia	7°16′11.53″ O; 37°30′34.09″ N	ISOD-12	4.72	17.2	0.1655	0.512342 (7)	−4.4	2547

References

1. Allen, R.L.; Weihed, P.; Blundell, D.; Crawford, T.; Davidson, G.; Galley, A.; Gibson, H.; Hannington, M.; Herzig, P.; Large, R.; et al. Global comparisons of volcanic-hosted massive sulphide districts. In *The Timing and Location of Major Ore Deposits in An Evolving Orogen*; Blundell, D., Neubauer, F., von Quadt, A., Eds.; The Geological Society: London, UK, 2002; pp. 13–37.
2. Piercey, S.J. Lithogeochemistry of Volcanic Rocks Associated with Volcanogenic Massive Sulphide Deposits and Applications to Exploration. In *Submarine Volcanism and Mineralization: Modern through Ancient*; Cousens, B., Piercey, S.J., Eds.; Geological Association of Canada: St. John's, NL, Canada, 2009; pp. 15–40.
3. Barrie, C.T.; Hannington, M.D. Classification of volcanic-associated massive sulfide deposits based on host-rock composition. In *Volcanic-Associated Massive Sulfide Deposits—Processes and Examples in Modern and Ancient Settings*; Barrie, C.T., Hannington, M.D., Eds.; Reviews in Economic Geology: Littleton, CO, USA, 1999; Volume 8, pp. 1–11.
4. Leistel, J.M.; Marcoux, E.; Thiéblemont, E.; Quesada, C.; Sánchez, A.; Almodóvar, G.R.; Pascual, E.; Saez, R. The volcanic-hosted massive sulphide deposits of the Iberian Pyrite Belt. *Miner. Depos.* **1998**, *33*, 2–30. [[CrossRef](#)]
5. Saez, R.; Pascual, E.; Toscano, M.; Almodovar, G.R. The Iberian type of volcano-sedimentary massive sulphide deposits. *Miner. Depos.* **1999**, *5–6*, 549–570. [[CrossRef](#)]
6. Tornos, F. Environment of formation and styles of volcanogenic massive sulfides: The Iberian Pyrite Belt. *Ore Geol. Rev.* **2006**, *28*, 259–307. [[CrossRef](#)]
7. Leshner, C.M.; Goodwin, A.M.; Campbell, I.H.; Gorton, M.P. Trace-element geochemistry of ore-associated and barren, felsic metavolcanic rocks in the Superior province, Canada. *Can. J. Earth Sci.* **1986**, *23*, 222–237. [[CrossRef](#)]
8. Barrie, C.T.; Ludden, J.N.; Green, T.H. Geochemistry of volcanic rocks associated with Cu-Zn and Ni-Cu deposits in the Abitibi Subprovince. *Econ. Geol.* **1993**, *88*, 1341–1358. [[CrossRef](#)]
9. Lentz, D.R. Petrogenetic evolution of felsic volcanic sequences associated with Phanerozoic volcanic-hosted massive sulphide systems: The role of extensional geodynamics. *Ore Geol. Rev.* **1998**, *12*, 289–327. [[CrossRef](#)]
10. Hart, T.R.; Gibson, H.L.; Leshner, M. Trace element geochemistry and petrogenesis of felsic volcanic rocks associated with volcanogenic massive Cu-Zn-Pb sulfide deposits. *Econ. Geol.* **2004**, *99*, 1003–1013. [[CrossRef](#)]
11. Piercey, S.J.; Peter, J.M.; Mortensen, J.K.; Paradis, S.; Murphy, D.C.; Tucker, T.L. Petrology and U-Pb geochronology of footwall porphyritic rhyolites from the Wolverine volcanogenic massive sulfide deposit, Yukon, Canada: Implications for the genesis of massive sulfide deposits in continental margin environments. *Econ. Geol.* **2008**, *103*, 5–33. [[CrossRef](#)]
12. Valenzuela, A.; Donaïre, T.; Pin, C.; Toscano, M.; Hamilton, M.; Pascual, E. Geochemistry and U-Pb dating of felsic volcanic rocks in the Riotinto-Nerva unit, Iberian Pyrite Belt, Spain: Crustal thinning, progressive crustal melting and massive sulphide genesis. *J. Geol. Soc.* **2011**, *168*, 717–731. [[CrossRef](#)]
13. Codeço, M.S.; Mateus, A.; Figueiras, J.; Rodrigues, P.; Gonçalves, L. Development of the Ervidel-Roxo and Figueirinha-Albernoa volcanic sequences in the Iberian Pyrite Belt, Portugal: Metallogenic and geodynamic implications. *Ore Geol. Rev.* **2018**, *98*, 80–108. [[CrossRef](#)]
14. Donaïre, T.; Pascual, E.; Saez, R.; Pin, C.; Hamilton, M.A.; Toscano, M. Geochemical and Nd isotopic signature of felsic volcanic rocks as a proxy of volcanic-hosted massive sulphide deposits in the Iberian Pyrite Belt (SW, Spain): The Paymogo Volcano-Sedimentary Alignment. *Ore Geol. Rev.* **2020**, *120*, 103408. [[CrossRef](#)]
15. Horikoshi, E. Volcanic activity related to the formation of the Kuroko-type deposits in the Kosaka district, Japan. *Miner. Depos.* **1969**, *4*, 321–345. [[CrossRef](#)]
16. Cas, R.A.F. Submarine volcanism: Eruption styles, products, and relevance to understanding the host-rock successions to volcanic-hosted massive sulfide deposits. *Econ. Geol.* **1992**, *87*, 511–541. [[CrossRef](#)]
17. Gibson, H.L.; Morton, R.L.; Hudak, G.J. Submarine volcanic processes, deposits, and environments favorable for the location of volcanic associated massive sulfide deposits. In *Volcanic-Associated Massive Sulfide Deposits: Processes and Examples in Modern and Ancient Settings*; Barrie, C.T., Hannington, M.D., Eds.; Reviews in Economic Geology; Society of Economic Geologists: Littleton, CO, USA, 1999; Volume 8, pp. 13–51.
18. Soriano, C.; Marti, J. Facies analysis of volcano-sedimentary successions hosting massive sulphide deposits in the Iberian Pyrite Belt, Spain. *Econ. Geol.* **1999**, *94*, 867–882. [[CrossRef](#)]
19. Allen, R.L.; Weihed, P.; Svenson, S. Setting of Zn-Cu-Au-Ag massive sulfide deposits in the evolution and facies architecture of a 1.9 Ga marine volcanic arc, Skellefte District, Sweden. *Econ. Geol.* **1997**, *91*, 1022–1053. [[CrossRef](#)]
20. McPhie, J.; Allen, R.L. Submarine, silicic, syn-eruptive pyroclastic units in the Mount Read Volcanics, western Tasmania: Influence of vent setting and proximity on lithofacies characteristics. In *Explosive Subaqueous Volcanism*; White, J., Smellie, J.L., Clague, D.A., Eds.; Geophysical Monograph Series; AGU: Washington, DC, USA, 2003; Volume 140, pp. 245–258.
21. Valenzuela, A.; Donaïre, T.; González-Roldán, M.; Toscano, M.; Pascual, E. Volcanic architecture in the Odiel river area and the volcanic environment in the Riotinto-Nerva Unit, Iberian Pyrite Belt, Spain. *J. Volcanol. Geotherm. Res.* **2011**, *202*, 29–46. [[CrossRef](#)]
22. Donaïre, T.; Pascual, E.; Saez, R.; Toscano, M. Facies architecture and palaeoenvironmental constraints of subaqueous felsic volcanism in the Iberian Pyrite Belt: The Paymogo Volcano-Sedimentary Alignment. *J. Volcanol. Geotherm. Res.* **2020**, *405*, 107045. [[CrossRef](#)]
23. Schermerhorn, L.J.G. An outline stratigraphy of the Iberian Pyrite Belt. *Bol. Geol. Min. España* **1971**, *82*, 23–52.

24. Moreno, C.; Sierra, S.; Saez, R. Evidence for catastrophism at the Famennian-Dinantian boundary in the Iberian Pyrite Belt. In *Recent Advances in Lower Carboniferous Geology*; Strogon, P., Sommerville, I.D., Jones, G.L., Eds.; Geological Society Special Publication: London, UK, 1997; Volume 107, pp. 153–162.
25. Boogaard, M.V.D.; Schermerhorn, L.J.G. Conodont faunas from Portugal and southwestern Spain. Part 4: Famennian conodont fauna near Nerva (Rio Tinto). *Scripta. Geol.* **1980**, *56*, 1–14.
26. Routhier, P.; Aye, F.; Boyer, C.; Lecolle, M.; Moliere, P.; Picot, P.; Roger, G. La ceinture sud-iberique a amas sulfures dans sa partie espagnole mediane. Tableau geologique et metallogenique. Synthese sur le type amas sulfures volcano-sedimentaires. *Mémoires BRGM* **1978**, *94*, 266.
27. Munhá, J.; Kerrich, R. Sea water-basalt interaction in spilites from the Iberian Pyrite Belt. *Contrib. Mineral. Petrol.* **1980**, *73*, 191–200. [[CrossRef](#)]
28. Mitjavila, J.; Martí, J.; Soriano, C. Magmatic evolution and tectonic setting of the Iberian Pyrite Belt volcanism. *J. Petrol.* **1997**, *38*, 727–755. [[CrossRef](#)]
29. Thiéblemont, D.; Pascual, E.; Stein, G. Magmatism in the Iberian Pyrite Belt: Petrological constraints on a metallogenetic model. *Miner. Depos.* **1998**, *33*, 98–110. [[CrossRef](#)]
30. Rosa, C.J.P.; McPhie, J.; Relvas, J.M.R.S. Type of volcanoes hosting the massive sulfide deposits of the Iberian Pyrite Belt. *J. Volcanol. Geotherm. Res.* **2010**, *194*, 107–126. [[CrossRef](#)]
31. Rosa, C.J.P.; McPhie, J.; Relvas, J.M.R.S.; Pereira, Z.; Oliveira, T.; Pacheco, N. Facies analyses and volcanic setting of the giant Neves Corvo massive sulfide deposit, Iberian Pyrite Belt, Portugal. *Miner. Depos.* **2008**, *43*, 449–466. [[CrossRef](#)]
32. Pereira, Z.; Saez, R.; Pons, J.M.; Oliveira, J.T.; Moreno, C. Edad devónica (Struniense) de las mineralizaciones de Aznalcóllar (Faja Pirítica Ibérica) en base a palinología. *Geogaceta* **1996**, *20*, 1609–1612.
33. González, F.; Playford, G.; Moreno, C. Upper Devonian biostratigraphy of the Iberian Pyrite Belt, southwest Spain. Part One: Miospores. *Palaeontogr. Abt.* **2005**, *273*, 1–51. [[CrossRef](#)]
34. Barrie, C.T.; Amelin, Y.; Pascual, E. U–Pb geochronology of VMS mineralisation in the Iberian Pyrite Belt. *Miner. Depos.* **2002**, *37*, 684–703. [[CrossRef](#)]
35. Silva, J.B.; Oliveira, J.T.; Ribeiro, A. Structural outline. South Portuguese Zone. In *Pre-Mesozoic Geology of Iberia*; Dallmeyer, R.D., Martínez García, E., Eds.; Springer: Berlin, Germany, 1990; pp. 348–363.
36. Oliveira, J.T. South Portuguese Zone: Introduction. Stratigraphy and synsedimentary tectonism. In *PreMesozoic Geology of Iberia*; Dallmeyer, R.D., Martínez García, E., Eds.; Springer: Berlin, Germany, 1990; pp. 333–347.
37. Moreno, C. Las facies Culm del Anticlinorio de Puebla de Guzmán (Huelva). Unpublished Ph.D. Thesis, University of Granada, Granada, Spain, 1986; 370p.
38. Mantero, E.M.; García Navarro, E.; Alonso-Chaves, F.M.; Martín Parra, L.M.; Matas, J.; Azor, J. La Zona Sudportuguesa: Propuesta para la división de un bloque continental en dominios. *Geogaceta* **2007**, *43*, 27–30.
39. Mantero, E.M.; Alonso-Chaves, F.M.; García-Navarro, E.; Azor, A. Tectonic style and structural analysis of the Puebla de Guzmán Antiform (Iberian Pyrite Belt, South Portuguese Zone, SW Spain). *Geol. Soc. Lond.* **2011**, *349*, 203–222. [[CrossRef](#)]
40. Rosa, C.J.P. Facies architecture of the Volcanic Sedimentary Complex of the Iberian Pyrite Belt, Portugal and Spain. Unpublished Ph.D. Thesis, University of Tasmania, Hobart, Australia, 2007; 357p.
41. Valenzuela, A.; Donaire, T.; Pascual, E. The Villanueva de los Castillejos section. In *Field Trip Guide “The Geology of the Volcanic-Hosted Massive Sulphide of the Iberian Pyrite Belt” GEODE–Global Comparison Massive Sulphide Project*; Tornos, F., Relvas, J.M.R.S., Almodóvar, G., Eds.; Aracena, Huelva, Spain, 2003; pp. 40–42.
42. Macías-Gutiérrez, G. Petrografía del Complejo Vulcano-Sedimentario en el sector de El Almendro-Villanueva de Los Castillejos (Faja Pirítica Ibérica). Unpublished BSc. Thesis, University of Huelva, Huelva, Spain, 2019; 41p.
43. McPhie, J.; Doyle, M.; Allen, R.L. *Volcanic Textures: A Guide to the Interpretation of Textures in Volcanic Rocks*; Centre for Ore Deposit and Exploration Studies, University of Tasmania: Hobart, Australia, 1993; 196p.
44. Ludwig, K.R. *User’s Manual for Isoplot 3.00 a Geochronological Toolkit for Microsoft Excel*; Special Publication Berkeley Geochronology Center: Berkeley, CA, USA, 2003; Volume 4, p. 74.
45. Pin, C.; Binon, M.; Belin, J.M.; Barbarin, B.; Clemens, J.D. Origin of microgranular enclaves in granitoids: Equivocal Sr–Nd evidence from Hercynian rocks in the Massif Central (France). *J. Geophys. Res.* **1990**, *95*, 17821–17828. [[CrossRef](#)]
46. Jacobsen, S.B.; Wasserburg, G.J. A two-reservoir recycling model for mantle-crustal evolution. *Geophysics* **1980**, *77*, 6298–6302.
47. Depaolo, D.J. Implication of correlated Nd and Sr isotopic variations for the chemical evolution of the crust and mantle. *Earth Planet. Sci. Lett.* **1979**, *43*, 201–211. [[CrossRef](#)]
48. Junta de Andalucía. *Project: Investigación Geológica y Cartografía Básica en la Faja Pirítica y Áreas Aledañas*; Junta de Andalucía & Instituto Geológico y Minero de España: Madrid, Spain, 1999.
49. Simancas, J.F. Geología de la extremidad oriental de la zona sudportuguesa. Unpublished Ph.D. Thesis, University of Granada, Granada, Spain, 1983; 439p.
50. Sáez, R.; Almodóvar, G.R.; Pascual, E. Geological constraints on massive sulphide genesis in the Iberian Pyrite Belt. *Ore Geol. Rev.* **1996**, *11*, 429–451. [[CrossRef](#)]
51. Winchester, J.A.; Floyd, P.A. Geochemical discrimination of different magma series and their differentiation products using immobile elements. *J. Chem. Geol.* **1977**, *20*, 325–343. [[CrossRef](#)]

52. Sun, S.S.; McDonough, W.F. Chemical and isotopic systematics of oceanic basalts; implications for mantle composition and processes. In *Magmatism in the Ocean Basins*; Saunders, A.D., Norry, M.J., Eds.; Geological Society of London: London, UK, 1989; Volume 42, pp. 313–345.
53. Nakamura, N. Determination of REE, Ba, Fe, Mg, Na, and K in carbonaceous and ordinary chondrites. *Geochim. Cosmochim. Acta* **1974**, *38*, 757–775. [[CrossRef](#)]
54. Tornos, F.; Clavijo, E.G.; Spiro, B. The Filon Norte orebody (Tharsis, Iberian Pyrite Belt): A proximal low-temperature shale-hosted massive sulphide in a thin-skinned tectonic belt. *Miner. Depos.* **1998**, *33*, 150–169. [[CrossRef](#)]
55. Simancas, J.F.; Carbonell, R.; González Lodeiro, F.; Pérez Estaún, A.; Juhlin, C.; Ayarza, P.; Kashubin, A.; Azor, A.; Martínez Poyatos, D.; Almodóvar, G.R.; et al. Crustal structure of the transpressional Variscan orogen of SW Iberia: SW Iberia deep seismic reflection profile (IBERSEIS). *Tectonics* **2006**, *22*, 1062. [[CrossRef](#)]
56. Almodóvar, G.R.; Sáez, R.; Pons, J.; Maestre, A.; Toscano, M.; Pascual, E. Geology and genesis of the Aznalcóllar ore deposits, Iberian Pyrite Belt, Spain. *Miner. Dep.* **1998**, *33*, 111–136.
57. Boulter, C.A.; Soriano, C.; Zimman, P. The Iberian Pyrite Belt: A mineralized system dismembered by voluminous high-level sills. *Terra Nova* **2001**, *13*, 99–104. [[CrossRef](#)]
58. Donaire, T.; Sáez, R.; Pascual, E. Rhyolitic globular peperites from the Aznalcóllar mining district (Iberian Pyrite Belt, Spain): Physical and chemical controls. *J. Volcanol. Geotherm. Res.* **2002**, *114*, 119–128. [[CrossRef](#)]
59. Cathles, L.M. An analysis of the hydrothermal system responsible for massive sulfide deposition in the Hokuroku basin of Japan. *Econ. Geol. Mon.* **1983**, *5*, 439–487.
60. Cathles, L.M.; Erendi, A.H.J.; Barrie, C.T. How long can a hydrothermal system be sustained by a single intrusive event? *Econ. Geol.* **1997**, *92*, 766–771. [[CrossRef](#)]
61. Jaffey, A.H.; Flynn, K.F.; Glendenin, L.F.; Bentley, W.C.; Easling, A.M. Precision measurements of half-lives and specific activities of ^{235}U and ^{238}U . *Phys. Rev. C* **1971**, *4*, 1889–1906. [[CrossRef](#)]